

Variable Winds and Dust Formation in R Coronae Borealis Stars

Geoffrey C. Clayton¹, T.R. Geballe², Wanshu Zhang¹

ABSTRACT

We have observed P-Cygni and asymmetric, blue-shifted absorption profiles in the He I $\lambda 10830$ lines of twelve R Coronae Borealis (RCB) stars over short (1 month) and long (3 year) timescales to look for variations linked to their dust-formation episodes. In almost all cases, the strengths and terminal velocities of the line vary significantly and are correlated with dust formation events. Strong absorption features with blue-shifted velocities ~ 400 km s⁻¹ appear during declines in visible brightness and persist for about 100 days after recovery to maximum brightness. Small residual winds of somewhat lower velocity are present outside of the decline and recovery periods. The correlations support models in which recently formed dust near the star is propelled outward at high speed by radiation pressure and drags the gas along with it.

Subject headings: dust – stars: carbon – stars: variable – line: formation – line: profiles

1. Introduction

The R Coronae Borealis (RCB) stars are a small group of carbon-rich, hydrogen-deficient, post-AGB supergiants. Almost 100 RCB stars are known in the Galaxy and the Magellanic Clouds (Clayton 1996, 2012; Tisserand et al. 2013). Two scenarios have been proposed for the origin of an RCB star: the double degenerate (DD) and the final helium-shell flash (FF) models (Iben et al. 1996). The former involves the merger of a CO- and a He-white dwarf (WD) (Webbink 1984). In the latter, a star evolving into a planetary nebula central star is blown up to supergiant size by a FF (Renzini 1979).

Their defining characteristic is unusual variability - RCB stars undergo massive declines of up to 8 mag due to the formation of carbon dust at irregular intervals. (Clayton 1996).

¹Department of Physics & Astronomy, Louisiana State University, Baton Rouge, LA 70803; gclayton,@fenway.phys.lsu.edu, wzhan21@lsu.edu

²Gemini Observatory, 670 N. A'ohoku Place, Hilo, HI 96720; tgeballe@gemini.edu

Typically the atmospheres of these stars are, $\sim 98\%$ helium, $\sim 1\%$ carbon, and almost no hydrogen (Asplund et al. 2000). It has been suggested that when dust forms around an RCB star, radiation pressure accelerates the dust away from the star, dragging gas along with it (Payne-Gaposchkin 1963; Clayton et al. 1992a). There is evidence for both low (10-20 km s $^{-1}$) and high (200-400 km s $^{-1}$) velocity gas streaming away from some RCB stars (Clayton et al. 1992a, 2003; García-Hernández et al. 2011). However, it is not known if wind speeds and mass loss rates are time-variable and if so how they depend on dust formation events.

Clayton et al. (2003) presented velocity-resolved spectra of the He I $2^3P - 2^3S$ $\lambda 10830$ line in RCB stars showing that most, if not all of them have winds. Nine of the ten stars observed showed P-Cygni or asymmetric blue-shifted line profiles. As ionization of He I requires photons of energies > 24 eV it is likely that the $n = 2$ levels of He I that produce this line are populated by collisions rather than by photoionization/recombination in these stars, whose effective temperatures imply very low far ultraviolet luminosities. The observed $\lambda 10830$ line profiles were modeled using a Sobolev plus Exact Integration (SEI) code to derive optical depths and velocity fields of the helium (Clayton et al. 2003). The fits imply that the helium in a typical RCB wind undergoes steep acceleration to a terminal velocity of $V_\infty = 200\text{-}350$ km s $^{-1}$ and has a column density of $N_{He} \sim 10^{12}$ cm $^{-2}$ in the metastable 2^3S level. Interestingly, the five known hydrogen-deficient carbon (HdC) stars, which are spectroscopically identical to the RCB stars, but produce no dust (i.e., do not vary in optical brightness), have also been observed at He I $\lambda 10830$ (Geballe et al. 2009). No evidence for a stellar wind was found in any of the five stars, consistent with the suspected dust – wind connection in this extended family of stars.

Clayton et al. (2003) suggested that there may be a relationship between the light curve of an RCB star and its He I $\lambda 10830$ profile, as the He I wind features were stronger when they were closer in time to a dust formation episode. Here we report on five epochs of He I $\lambda 10830$ spectra of twelve RCB stars, obtained over a three year period. We use these data to study how the equivalent widths and terminal velocities of the line vary with time and to determine more quantitatively if those variations are related to the timing of dust formation episodes.

2. Observations and Data Reduction

Observations of He I $\lambda 10830$ in twelve RCB stars were obtained on six nights of highly variable weather conditions between 2001 June and 2004 July at the United Kingdom Infrared Telescope (UKIRT) using its facility spectrometer CGS4 configured with its echelle

grating and two-pixel ($0''.9$) wide slit. The observations are summarized in Table 1. The resolution was $5 \times 10^{-5} \mu\text{m}$ (14 km s^{-1}). The spectra were ratioed with those of nearby A stars in order to remove telluric features. Wavelength calibration was achieved using telluric absorption lines observed in the comparison stars. A quadratic fit was made to a selection of these lines covering the entire spectral range. The $1\text{-}\sigma$ wavelength uncertainty is $5\text{-}8 \times 10^{-6} \mu\text{m}$. The spectra have been corrected for each star’s radial velocity, and a heliocentric correction has also been made based on the epoch of each observation. Thus, in the final reduced spectra the wavelength scale (*in vacuo*) refers to the rest frame of the star and the wavelength of the He I $\lambda 10830$ line is $1.08333 \mu\text{m}$ (Geballe et al. 2009). One star, ES Aql, does not have a published radial velocity. A value of -70 km s^{-1} has been inferred for it from the spectra analyzed here. The stellar radial velocities used for this study are listed in Table 1.

The normalized spectra, slightly smoothed to a resolution of $6.5 \times 10^{-5} \mu\text{m}$ (18 km s^{-1}), are shown in Fig. 1. In most cases the helium line dominates the spectral region. The wavelengths of the other prominent atomic lines are indicated in the figure. Many other absorption lines are present. The signal-to-noise ratio exceeds 50 in most cases, but in some spectra (V854 Cen, 3rd spectrum from top, (UX Ant, all spectra; WX CrA, top spectrum; V517 Oph, top spectrum; U Aqr, all spectra; ES Aql, top spectrum; SV Sge, top spectrum) the noise level can be estimated from the fluctuations between strong spectral features.

As listed in Table 1, the RCB stars range in effective temperature (T_{eff}) from 4000 to 7500 K. Their spectra have very different appearances depending on whether T_{eff} is greater than or less than $\sim 6000 \text{ K}$ (Asplund et al. 2000). The warmer stars, plotted in Figure 1a, show mainly atomic absorptions of C I and singly ionized metals while the cooler stars, in Figure 1b, show in addition, strong C_2 and CN absorption bands. The line identifications are from Hirai (1974), and Hinkle et al. (1995). Two stars, ES Aql and V517 Oph, do not have reported values of T_{eff} , but their spectra resemble those of RCB stars with $T_{eff} \sim 5000 \text{ K}$. Note that each panel in Fig. 1 contains a model RCB stellar spectrum, of either a 5400 K or a 6500 K RCB star (Geballe et al. 2009; García-Hernández et al. 2009) depending on which is more appropriate to the effective temperature of the star.

Light curves of the sample stars for the time period of the He I observations are shown in Fig. 2. They consist of visual data downloaded from the AAVSO International Database (Henden, A.A., 2008, private communication), and V-band data from the ASAS-3 telescope (Pojmanski 2002). The epochs at which He I $\lambda 10830$ spectra were obtained for each star, listed in Table 1, are marked on the light curves.

The equivalent widths (EW) and terminal velocity (v_∞) of the blue-shifted absorption in the He I $\lambda 10830$ line were measured for each spectrum. They are listed in Table 2.

The wavelength range for which the EW was calculated was determined by comparing each spectrum to model RCB stellar spectra. The EW was corrected to the extent possible for stellar absorption lines, in particular for the Si I line at $1.0830 \mu\text{m}$. In a few spectra, an absorption could not be measured because strong emission extended over a wide velocity range and/or the continuum was too weak to reliably measure absorption. For all other spectra, the absorption EW and v_∞ for each epoch is plotted against the time in days since the end of that star’s latest decline (also listed in Table 2) in Fig. 3, with the values of those quantities during the decline shown on the left hand edges of the plots. Note that the filled symbols in Fig. 3 comprise the data for all but two of the stars, whereas the open symbols apply to two unusual cases, V482 Cyg and V854 Cen.

3. Discussion

3.1. Previous Observations of He I $\lambda 10830$

Blue-shifted high-velocity absorption features ($100\text{--}400 \text{ km s}^{-1}$) have been reported from time to time in the spectra of RCB stars, observed at early and late times during declines (Alexander et al. 1972; Cottrell et al. 1990; Clayton et al. 1992b, 1993, 1994; Vanture & Wallerstein 1995; Goswami et al. 1997; Rao & Lambert 1997). For example, the Na I D lines in R CrB showed blue-shifted absorption during that star’s recovery from its 1995-96 decline (Rao et al. 1999). The line profiles implied that the gas was being accelerated from 100 to 200 km s^{-1} . During its 2003 minimum, R CrB showed blue wings in the infrared O I triplet lines implying ejection at 130 km s^{-1} (Rao et al. 2006). However, a blue wing was also present at maximum light. A similar ejection velocity in V CrA was also determined from its O I line profiles (Rao & Lambert 2008).

Prior to the small survey by Clayton et al. (2003), very few observations of the He I $\lambda 10830$ line in RCB stars had been reported. R CrB, itself, however, was observed at five epochs between 1972 and 1978, and showed a P-Cygni or asymmetric blue-shifted profile at all times, whether in decline or at maximum light (Wing et al. 1972; Querci & Querci 1978; Zirin 1982). R CrB showed emission at He I $\lambda 10830$ in three spectra obtained during a decline in 1972 March–May when it was between $V = 9$ and 12 mag (Wing et al. 1972). On 1977 January 18 at $V = 7.0$, during recovery after a decline, the line had a P-Cygni profile with $v_\infty = -240 \text{ km s}^{-1}$ (Querci & Querci 1978). On 1978 July 24, R CrB showed very strong absorption at He I $\lambda 10830$ with a velocity shift of $\sim -200 \text{ km s}^{-1}$, several months after it had returned to maximum light after a decline (Zirin 1982). The helium-final-flash star, Sakurai’s Object, which may be related to the RCB stars, showed an increasingly blue-shifted absorption out to 670 km s^{-1} at He I $\lambda 10830$ as the star formed dust and went into

a deep RCB-like decline (Eyres et al. 1999), from which it has yet to recover.

3.2. New Observations

Temporal correlations between dust obscuration and He I $\lambda 10830$ line properties associated with wind activity can be discerned by comparing the individual observed spectra in Fig. 1 to the individual light curves in Fig. 2, or collectively by examination of Fig. 3, in which the key line parameters, absorption strength, and terminal velocity are presented for all of the stars on a single time axis whose origin is the end of the most recent decline of each star. Viewed collectively, as in Fig. 3, the data reveal a fairly uniform behavioral pattern. There is a strong correlation between visual obscuration and the strength of the blue-shifted He I $\lambda 10830$ absorption, with increased obscuration associated with a large increase in the line strength. There also is a clear tendency for the maximum velocity of the wind to be greater during a decline than well after it has ended.

Even small episodes of dust formation, such as that seen in V CrA on \sim JD 2452800 (Fig. 2), are coincident with significant increases in wind activity. V CrA had declined visually by only ~ 0.5 mag but the EW of the wind features (the 2nd and 3rd spectra from the top in Fig. 1) increased greatly. There is some indication that the cooler RCB stars in the sample, V517 Oph, ES Aql, SV Sge and WX CrA have larger equivalent widths in He I during declines than the warmer stars. However, this might be due to sampling statistics, as a higher fraction of He I spectra of cool RCB stars were obtained during deep declines than for the warm RCB stars. There is also a tendency for a star in a deep decline, such that the stellar continuum is weak relative to the He I line emission, to show a classic P-Cygni profile in the $\lambda 10830$ line. This can be seen in Fig. 1b for WX CrA and U Aqr. In the last two spectra of SV Sge, the star was deep in a decline, and so had no continuum for an absorption to be seen against, but it showed strong He I $\lambda 10830$ emission.

Figure 3 reveals that the strength of the wind absorption drops off sharply beginning about 100 days after the end of a decline; that is, well after the star has returned to maximum brightness and there is ostensibly no dust along the line of sight. The same behavior is seen in the maximum velocity of the wind; it does not decrease significantly from its value during the decline of $300\text{--}400$ km s $^{-1}$ until after ~ 100 days. The latter behavior may not be surprising as high velocity gas far from the star may be expected to decelerate slowly. However, as most of the absorption is expected to occur in the densest part of the wind, closest to the star, one might predict the drop-off in absorption strength to commence very quickly after dust formation ceases and to decrease gradually thereafter.

Note, however, that even small episodes of dust formation profoundly affect the wind properties, as seen in V CrA. Thus it may be that sufficient dust continues to form and accelerate the gas during this ~ 100 -day interval. It is sometimes difficult to distinguish between pulsations and small dust formation episodes (e.g., Fernie & Lawson 1993; Clayton et al. 1995). More accurate photometry might be able to reveal this.

An additional noteworthy result is that a weak blueshifted He I λ 10830 line is present and roughly constant in strength in all of the stars in the sample even well beyond 100 days after each star's most recent decline. This implies the existence of a weak high velocity wind at all times and generalizes the conclusion drawn from historical observations of R CrB that a wind is always present, as discussed earlier. The constancy of this residual wind may suggest that a small amount of dust formation is always taking place.

The He I spectra in our sample that were obtained, by chance, just before a decline are sparse, but suggest that there are no precursive indications of changes in the line prior to a decline. The best examples are the two spectra of RY Sgr at \sim JD 2453150 (about 100 days before a decline), neither of which shows an increasing wind feature.

There are two exceptions to the general behavior described above: V854 Cen and V482 Cyg, whose line parameters are plotted separately from the other RCB stars in Fig. 3. V854 Cen, in particular, appears to behave differently. It had more dust formation episodes than any of the other RCB stars during 2001–2004. One might have expected, based on the behavior of the majority stars, that its wind features would therefore be very strong. Instead the opposite was observed: its spectrum has almost no He I λ 10830 absorption at the end of one decline (\sim JD 2452100), has modest absorption (albeit highly blueshifted) at the end of another decline (\sim JD 2452800), and again little or no absorption a month later. Unfortunately, no line measurements of V854 Cen were made when deep in a decline. In Figure 3, it can be seen that V854 Cen's terminal velocity, when measurable, is considerably higher than the other RCB stars. The rapid disappearance of its He I λ 10830 absorption after a dust formation episode could be attributed in part to that. V854 Cen is often the odd man out among RCB stars (Clayton 1996, 2012). It has a relatively large hydrogen abundance even though it is still hydrogen deficient, and has unusual abundances for an RCB star (Asplund et al. 1998, 2000).

V482 Cyg is the only star in the sample to show no dust formation activity during the epoch of He I observations, and it was already 1100 d past its last decline when the first He I λ 10830 spectra were obtained. Its line has the smallest measured EW in the sample. V482 Cyg is an extreme example of the general behavior, showing that a small residual wind is present even years after the latest decline.

3.3. Dust-Driven Winds in RCB Stars

In this section, we discuss the origin of the winds in RCB stars. We use simple equations to derive estimates of the mass-loss rate and wind terminal velocity, and compare those estimates to our own and other results, showing that models in which dust accelerates the gas and collisionally excites the lowest levels of the helium triplet state are consistent with the observations.

The lower state of the He I $\lambda 10830$ ($2^3S - 2^3P$) transition is more than 20 eV above the ground state. The transition probability is very small ($A_{21}=1.27 \times 10^{-4} \text{ s}^{-1}$) (Sasselov & Lester 1994). This metastable state could be populated by one of two mechanisms, photoionization/recombination or collisional excitation. He II $\lambda 1640$ is not seen in RCB stars which indicates that the He I $\lambda 10830$ line is not being formed by helium photoionization and recombination (Rossano et al. 1994; Clayton 1996; Lawson et al. 1999). R CrB, itself, showed emission lines of He I $\lambda\lambda$ 3889, 5876, 7065 and 10830 Å during the 1995-96 decline of R CrB (Rao et al. 1999). At the time of the observations, the 5876 Å line was much weaker than the 3889 and 7065 Å lines, which makes sense if the lines are optically thick and the electron density is high. Rao et al. (1999) estimate $T \sim 20000 \text{ K}$ and $n_e = 10^{11}-10^{12} \text{ cm}^{-3}$ so collisional excitation is important. In the final-flash star, Sakurai’s object, thought to be similar to RCB stars, the He I $\lambda 10830$ emission may be the result of collisional excitation in shocked gas being dragged outward by the expanding dust cloud around the star (Eyres et al. 1999; Tyne et al. 2000). The kinetic energy of a 400 km s^{-1} He atom is $\sim 3200 \text{ eV}$, which is 160 times the excitation energy of the 2^3S and 2^3P triplet levels, so as the He is accelerated by the dust, 20 eV collisional energy transfers exciting it to the triplet states are quite plausible. Collisions with relative velocities $> \sim 30 \text{ km s}^{-1}$ will have enough energy to excite the He atoms.

Dust can form anywhere around an RCB star, but a decline in brightness only occurs when dust forms along the line of sight. The blue-shifted absorption seen in He I $\lambda 10830$ is created in gas that also is along the line of sight. The two phenomena are thus caused by gas and dust located together in the same column toward the star and it is quite likely that they are related. An inspection of Fig. 2 shows that the RCB stars in the sample had a wide range of dust formation activity during the time period of the He I measurements. Some RCB stars are more active in general than others, but each star also shows changes in its level of dust formation activity on timescales no longer than several years (Jurcsik 1996; Clayton 1996).

Generally, the maximum possible mass-loss rate, \dot{M}_o , due to radiation pressure on dust grains is,

$$\dot{M}_o = \frac{L_\star}{cv_\infty} \quad (1)$$

where L_\star is the stellar luminosity and v_∞ is the terminal velocity (e.g., Knapp et al. 1982). But, if the optical depth of dust is large, then multiple scattering becomes important and,

$$\dot{M} = \dot{M}_o \tau_\infty \quad (2)$$

where τ_∞ is the total optical depth of the circumstellar dust (Gail & Sedlmayr 1986).

A warm RCB star like R CrB, itself, with $M_V = -5$ mag, has $L_\star \sim 10^4 L_\odot$ and $R_\star \sim 70 R_\odot$ (Clayton 2012). From Figure 3, a typical terminal velocity is $v_\infty = 400 \text{ km s}^{-1}$. So $\dot{M}_o \sim 5 \times 10^{-7} M_\odot \text{ yr}^{-1}$. An RCB star decline can be 8 mag below maximum at V, so assuming $\tau_\infty \sim 8$, then $\dot{M} = 4 \times 10^{-6} M_\odot \text{ yr}^{-1}$. This agrees well with estimates of RCB star mass loss from observations of R CrB, itself (Clayton et al. 2011, and references therein).

The radiation pressure on a spherical dust grain is,

$$F_{pr} = \frac{L_\star a^2 Q_{pr}}{4cr^2} \quad (3)$$

where Q_{pr} is the radiation pressure efficiency and r is the distance from the center of the star (Marsh 1976). Then, integrating from $r = r_o$, the condensation radius of the dust, to $r = \infty$ and from $v = 0$ to $v = v_\infty$ produces,

$$v_\infty = \left(\frac{3 \left(\frac{m_d}{m_g} \right) L_\star Q_{pr}}{8\pi a \rho_s c r_o} \right)^{1/2} \quad (4)$$

where $\frac{m_d}{m_g}$ is the mass dust-to-gas ratio, and a and ρ_s are the radius and density of the dust grains. The inclusion of the dust-to-gas ratio takes into account the momentum transfer from the dust to the much more massive He gas. RCB stars are $\sim 98\%$ He (Asplund et al. 2000).

If the dust is amorphous carbon, then $\rho_s \sim 2 \text{ g cm}^{-3}$. Assuming that $Q_{pr} = 1$, and $r_o = 2 R_\star = 1 \times 10^{13} \text{ cm}$ (Clayton 1996), and a typical dust-to-gas ratio for the Galaxy of 0.01 (Draine et al. 2007), then, $v_\infty = 2.8 \text{ a}^{-1/2}$. So, if a dust grain radius is $\sim 0.5 \mu\text{m}$, then $v_\infty \sim 400 \text{ km s}^{-1}$, which is typical for v_∞ measured from He I $\lambda 10830$ in this paper. This is slightly larger than other estimates of grain sizes around RCB stars (e.g., Evans et al. 1985; Fadeev

1988). But the dust grain size inferred here is consistent with other estimates considering that other parameters in Equation 4, such as the dust-to-gas ratio, the stellar luminosity, and the dust condensation radius are also somewhat uncertain.

4. Conclusions

The current data, although difficult to interpret for individual RCB stars due to the small number of observations per star, collectively they show a consistent behavioral pattern for the overwhelming majority of stars in the sample. At maximum light, most RCB stars show weak and highly blue-shifted ($\sim 200 \text{ km s}^{-1}$) He I $\lambda 10830$ line absorption from the excited 2^3S state, while at the same time producing a photospheric spectrum that is unshifted in the rest-frame of the star. Each decline in optical brightness coincides with an large increase in the He I $\lambda 10830$ line EW, coupled with an increase in v_∞ of the wind to $\sim 400 \text{ km s}^{-1}$. Following recovery to the pre-decline brightness, both the higher v_∞ and the increased EW persist for ~ 3 months before returning to their original pre-decline values. This strong correlation between dust formation and the blue-shifted absorption in He I $\lambda 10830$ is supported by the observations of the HdC stars, which are identical to the RCB stars spectroscopically, but produce no dust and have no evidence for blue-shifted absorption in He I $\lambda 10830$ (Geballe et al. 2009). So, in the RCB stars, helium gas is dragged along by dust grains accelerated by radiation pressure from the star.

The close connection between dust formation and this type of wind behavior provides strong support for the long held view that radiation pressure accelerates the newly formed dust and that it in turn collisionally excites the gas. The escape velocity from RCB is estimated to be $30\text{-}70 \text{ km s}^{-1}$ (Rao & Lambert 1997). Thus, the observed maximum velocities greatly exceed the escape velocities from these stars. A simple explanation for the presence of a (much weaker) wind in between declines is that a lower level of dust formation than observed in the declines is always taking place.

García-Hernández et al. (2011) have found evidence in the optical spectrum of scattered light from R CrB for dust velocities of only $\sim 25 \text{ km s}^{-1}$. That dust cannot be connected with the much higher velocities inferred from the He I $\lambda 10830$ line profile. The scattering may occur in dust located much further from the star than the dust responsible for the simultaneous strong obscuration of the starlight and acceleration of the gas, perhaps where the dust either has been greatly decelerated or where large quantities of dust ejected long ago at lower velocities have accumulated. R CrB has a large dust shell around it that may be a fossil planetary nebula shell (Clayton et al. 2011). In view of the above estimate of escape velocity, gas and dust ejected at low velocities from the star probably would not travel far

before being significantly decelerated and perhaps fall back into the star.

Additional observations of the He λ 10830 line, probably in the form of a more intensive campaign than the one reported here, combined with more accurate photometry are now needed to more stringently test and refine our conclusions.

We thank the anonymous referee for several helpful comments. We thank the staff of the United Kingdom Infrared Telescope, which is operated by the Joint Astronomy Centre on behalf of the U.K. Particle Physics and Astronomy Research Council. We acknowledge with thanks the variable star observations from the AAVSO International Database contributed by observers worldwide and used in this research. TRG's research is supported by the Gemini Observatory, which is operated by the Association of Universities for Research in Astronomy, Inc., on behalf of the international Gemini partnership of Argentina, Australia, Brazil, Canada, Chile, the United Kingdom, and the United States of America.

REFERENCES

- Alexander, J. B., Andrews, P. J., Catchpole, R. M., Feast, M. W., Lloyd Evans, T., Menzies, J. W., Wisse, P. N. J., & Wisse, M. 1972, *MNRAS*, 158, 305
- Asplund, M., Gustafsson, B., Kameswara Rao, N., & Lambert, D. L. 1998, *A&A*, 332, 651
- Asplund, M., Gustafsson, B., Kiselman, D., & Eriksson, K. 1997, *A&A*, 318, 521
- Asplund, M., Gustafsson, B., Lambert, D. L., & Rao, N. K. 2000, *A&A*, 353, 287
- Bergeat, J., Knapik, A., & Rutily, B. 2001, *A&A*, 369, 178
- Clayton, G. C. 1996, *PASP*, 108, 225
- . 2012, *JAAVSO*, 40, 539
- Clayton, G. C., Geballe, T. R., & Bianchi, L. 2003, *ApJ*, 595, 412
- Clayton, G. C., Lawson, W. A., Cottrell, P. L., Whitney, B. A., Stanford, S. A., & de Ruyter, F. 1994, *ApJ*, 432, 785
- Clayton, G. C., Lawson, W. A., Whitney, B. A., & Pollacco, D. L. 1993, *MNRAS*, 264, L13
- Clayton, G. C., Whitney, B. A., Meade, M. R., Babler, B., Bjorkman, K. S., & Nordsieck, K. H. 1995, *PASP*, 107, 416

- Clayton, G. C., Whitney, B. A., Stanford, S. A., & Drilling, J. S. 1992a, *ApJ*, 397, 652
- Clayton, G. C., Whitney, B. A., Stanford, S. A., Drilling, J. S., & Judge, P. G. 1992b, *ApJ*, 384, L19
- Clayton, G. C., et al. 2011, *ApJ*, 743, 44
- Cottrell, P. L., Lawson, W. A., & Buchhorn, M. 1990, *MNRAS*, 244, 149
- Draine, B. T., et al. 2007, *ApJ*, 663, 866
- Evans, A., Whittet, D. C. B., Davies, J. K., Kilkenny, D., & Bode, M. F. 1985, *MNRAS*, 217, 767
- Eyres, S. P. S., Smalley, B., Geballe, T. R., Evans, A., Asplund, M., & Tyne, V. H. 1999, *MNRAS*, 307, L11
- Fadeev, I. A. 1988, *MNRAS*, 233, 65
- Fernie, J. D., & Lawson, W. A. 1993, *MNRAS*, 265, 899
- Gail, H.-P., & Sedlmayr, E. 1986, *A&A*, 161, 201
- García-Hernández, D., Kameswara Rao, N., & Lambert, D. L. 2011, *ApJ*, 739, 37
- García-Hernández, D. A., Hinkle, K. H., Lambert, D. L., & Eriksson, K. 2009, *ApJ*, 696, 1733
- Geballe, T. R., Rao, N. K., & Clayton, G. C. 2009, *ApJ*, 698, 735
- Goswami, A., Rao, N. K., Lambert, D. L., & Gonzalez, G. 1997, *PASP*, 109, 796
- Hinkle, K., Wallace, L., & Livingston, W. 1995, *PASP*, 107, 1042
- Hirai, M. 1974, *PASJ*, 26, 163
- Iben, Jr., I., Tutukov, A. V., & Yungelson, L. R. 1996, *ApJ*, 456, 750
- Jurcsik, J. 1996, *Acta Astronomica*, 46, 325
- Kilkenny, D., Lloyd Evans, T., Bateson, F. M., Jones, A. F., & Lawson, W. A. 1992, *The Observatory*, 112, 158
- Knapp, G. R., Phillips, T. G., Leighton, R. B., Lo, K. Y., Wannier, P. G., Wootten, H. A., & Huggins, P. J. 1982, *ApJ*, 252, 616

- Lawson, W. A., & Cottrell, P. L. 1989, MNRAS, 240, 689
- . 1997, MNRAS, 285, 266
- Lawson, W. A., et al. 1999, AJ, 117, 3007
- Marsh, K. A. 1976, ApJ, 203, 552
- Payne-Gaposchkin, C. 1963, ApJ, 138, 320
- Pojmanski, G. 2002, Acta Astronomica, 52, 397
- Querci, M., & Querci, F. 1978, A&A, 70, L45
- Rao, N. K., & Lambert, D. L. 1993, PASP, 105, 574
- . 1997, MNRAS, 284, 489
- . 2003, PASP, 115, 1304
- . 2008, MNRAS, 384, 477
- Rao, N. K., Lambert, D. L., & Shetrone, M. D. 2006, MNRAS, 370, 941
- Rao, N. K., et al. 1999, MNRAS, 310, 717
- Renzini, A. 1979, in ASSL Vol. 75: Stars and star systems, ed. B. E. Westerlund, 155
- Rossano, G. S., Rudy, R. J., Puetter, R. C., & Lynch, D. K. 1994, AJ, 107, 1128
- Sasselov, D. D., & Lester, J. B. 1994, ApJ, 423, 785
- Tisserand, P., Clayton, G. C., Welch, D. L., Pilecki, B., Wyrzykowski, L., & Kilkenney, D. 2013, A&A, 551, A77
- Tyne, V. H., Eyres, S. P. S., Geballe, T. R., Evans, A., Smalley, B., Duerbeck, H. W., & Asplund, M. 2000, MNRAS, 315, 595
- Vanture, A. D., & Wallerstein, G. 1995, PASP, 107, 244
- Webbink, R. F. 1984, ApJ, 277, 355
- Wilson, R. E. 1953, Carnegie Institute Washington D.C. Publication, 0
- Wing, R. F., Baumert, J. H., Strom, S. E., & Strom, K. M. 1972, PASP, 84, 646
- Zirin, H. 1982, ApJ, 260, 655

Table 1. UKIRT Observations

Star	T_{eff}^a	RV^b	2001 June 15	2003 May 2	2003 June 2	2004 May 6	2004 June 4	2004 July 17
RY Sgr	7250	-20.5	X	X	X	X	X	
UX Ant	7000	+144.3			X	X	X	
R CrB	6750	+22.3	X	X	X	X	X	
V2552 Oph	6750	+60.5			X	X	X	
V854 Cen	6750	-25.1	X	X	X	X	X	
V482 Cyg	6500	-41.2	X	X	X	X	X	
V CrA	6250	-7.9	X	X	X	X	X	
U Aqr	6000	+98.0	X		X	X	X	X
WX CrA	5300	-3.8	X			X	X	
ES Aql	~5000	-70.0	X	X	X	X	X	
V517 Oph	~5000	+21.0	X	X	X	X	X	
SV Sge	4000	+4.0	X	X	X	X	X	

^a(Asplund et al. 1997, 1998, 2000; Bergeat et al. 2001; Rao & Lambert 2003). The effective temperatures of ES Aql and V517 Oph have never been calculated, but both show spectra indicative of cool RCB stars.

^b(Wilson 1953; Lawson & Cottrell 1989; Kilkenny et al. 1992; Rao & Lambert 1993; Lawson & Cottrell 1997; Rao & Lambert 2003)

Table 2. Measurements

Star	Epoch ^a	Days ^b	EW (Å)	V _∞
RY Sgr	1	0	5.5	-345
	2	686	1.2	-258
	3	717	1.0	-259
	4	1056	1.0	-250
	5	1085	1.2	-257
UX Ant	3	0	4.5	-420
	4	231	2.3	-408
	5	260	2.6	-417
R CrB	1	126	5.1	-392
	2	11	6.6	-427
	3	42	4.9	-413
	4	381	1.1	-313
	5	410	0.9	-303
V2552 Oph	3	292	1.8	-182
	4	631	2.1	-198
	5	660	1.9	-186
V854 Cen	1	0	1.0	-716
	2	11	5.1	-605
	3	42	2.0	-611
	4	381	1.3	-718
	5	410	0.7	-604
V482 Cyg	1	1376	0.9	-225
	2	1476	0.0	...
	3	1507	1.0	-179
	4	2431	0.9	-179
	5	2460	0.9	-218
V CrA	1	826	1.3	-366
	2	0	6.0	-397
	3	0	6.4	-435
	4	131	1.5	-346
	5	160	1.1	-304

Table 2—Continued

Star	Epoch ^a	Days ^b	EW (Å)	V _∞
U Aqr	1	0	4.3	-238
	3	0	6.3	-285
	4	0	4.6	-288
	5	0	5.4	-275
	6	0	5.8	-276
	WX CrA	1	0	7.7
4		0	5.6	-382
5		0	6.6	-383
ES Aql	1	0	5.2	-367
	2	0	10.2	-444
	3	0	10.2	-432
	4	0	11.0	-400
	5	0	11.2	-433
V517 Oph	1	0	9.8	-507
	2	61	6.2	-409
	3	92	6.9	-412
	4	0	9.3	-414
	5	0	10.7	-510
SV Sge	1	0	5.8	-312
	2	161	3.4	-315
	3	192	5.3	-313
	4	0
	5	0

^aThe epoch numbers refer to the six epochs in Table 1.

^bDays since the end of the last decline.

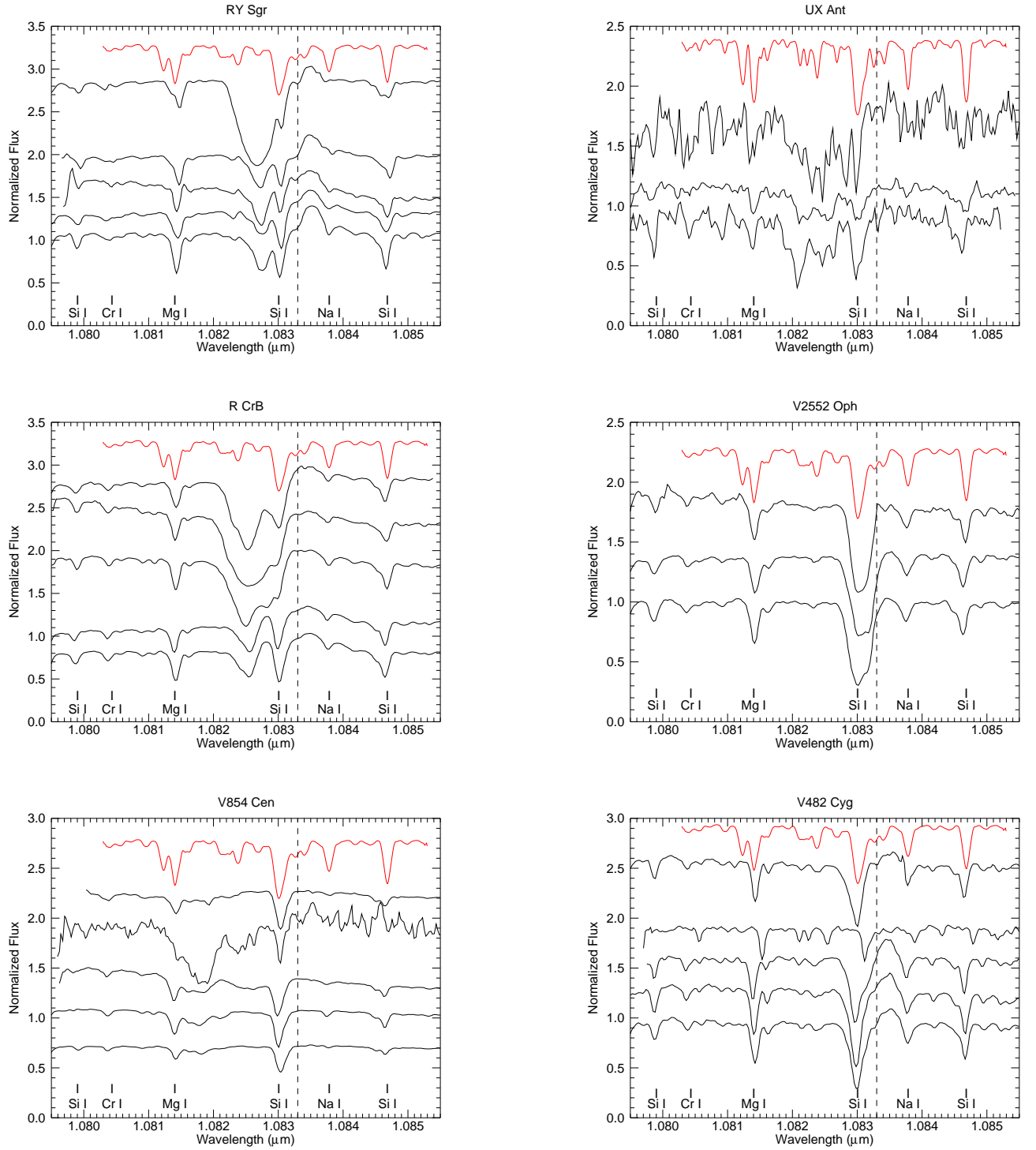


Fig. 1a.— UKIRT CGS4 echelle spectra in the region of the He I $\lambda 10830$ line. Vacuum wavelengths are plotted. The vertical dashed line shows the wavelength, $1.08333 \mu\text{m}$, of the He I $\lambda 10830$ (Geballe et al. 2009). In each panel individual normalized spectra are shifted vertically and are in chronological order from top to bottom. The epochs for each star are listed in Table 1. The red spectrum at the top of each panel is a 6500 K RCB stellar model (Geballe et al. 2009; García-Hernández et al. 2009).

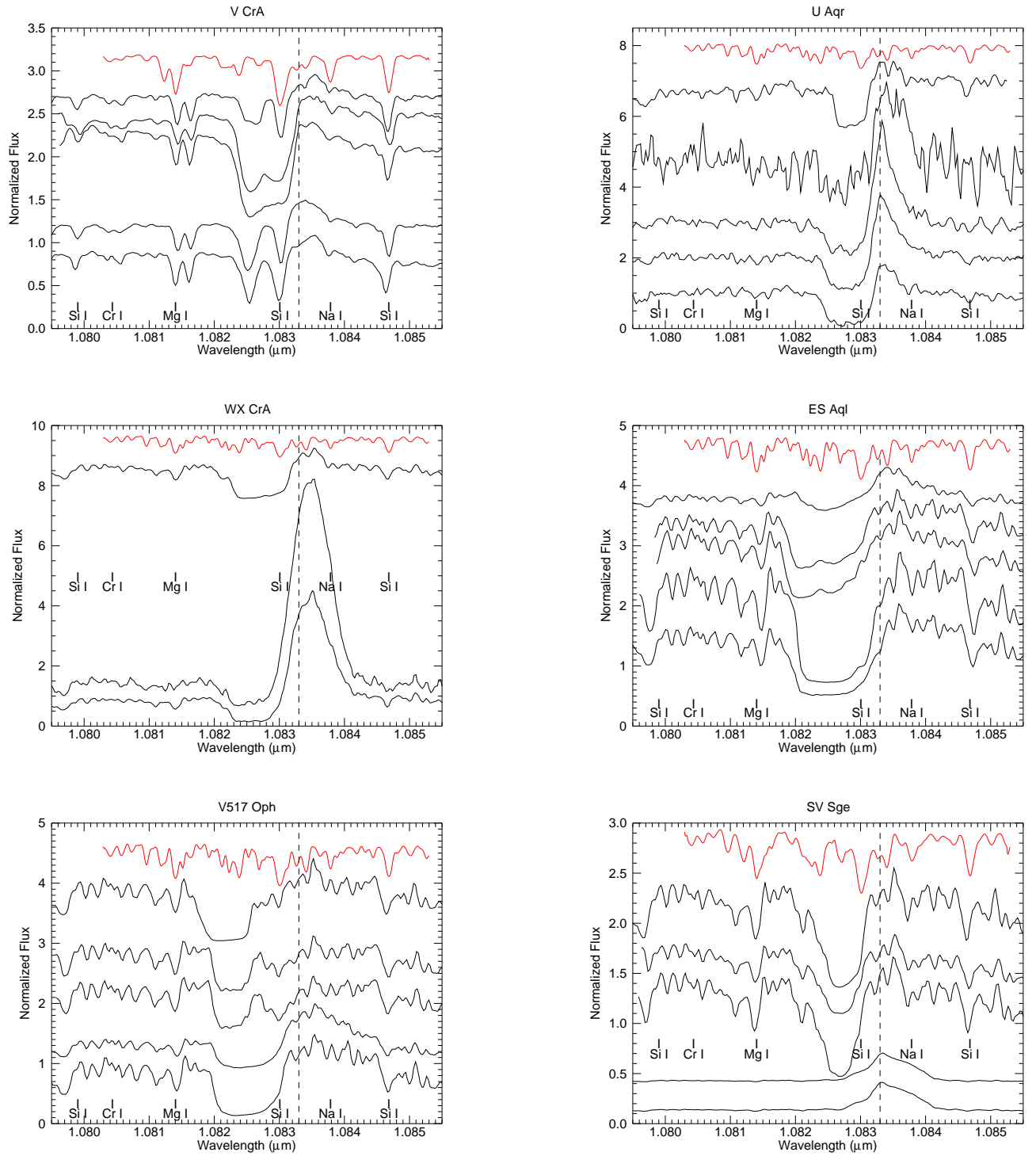


Fig. 1b.— Same as Fig. 1a, except that red spectrum is a 5400 K RCB stellar model except for V CrA which shows the 6500 K RCB model spectrum.

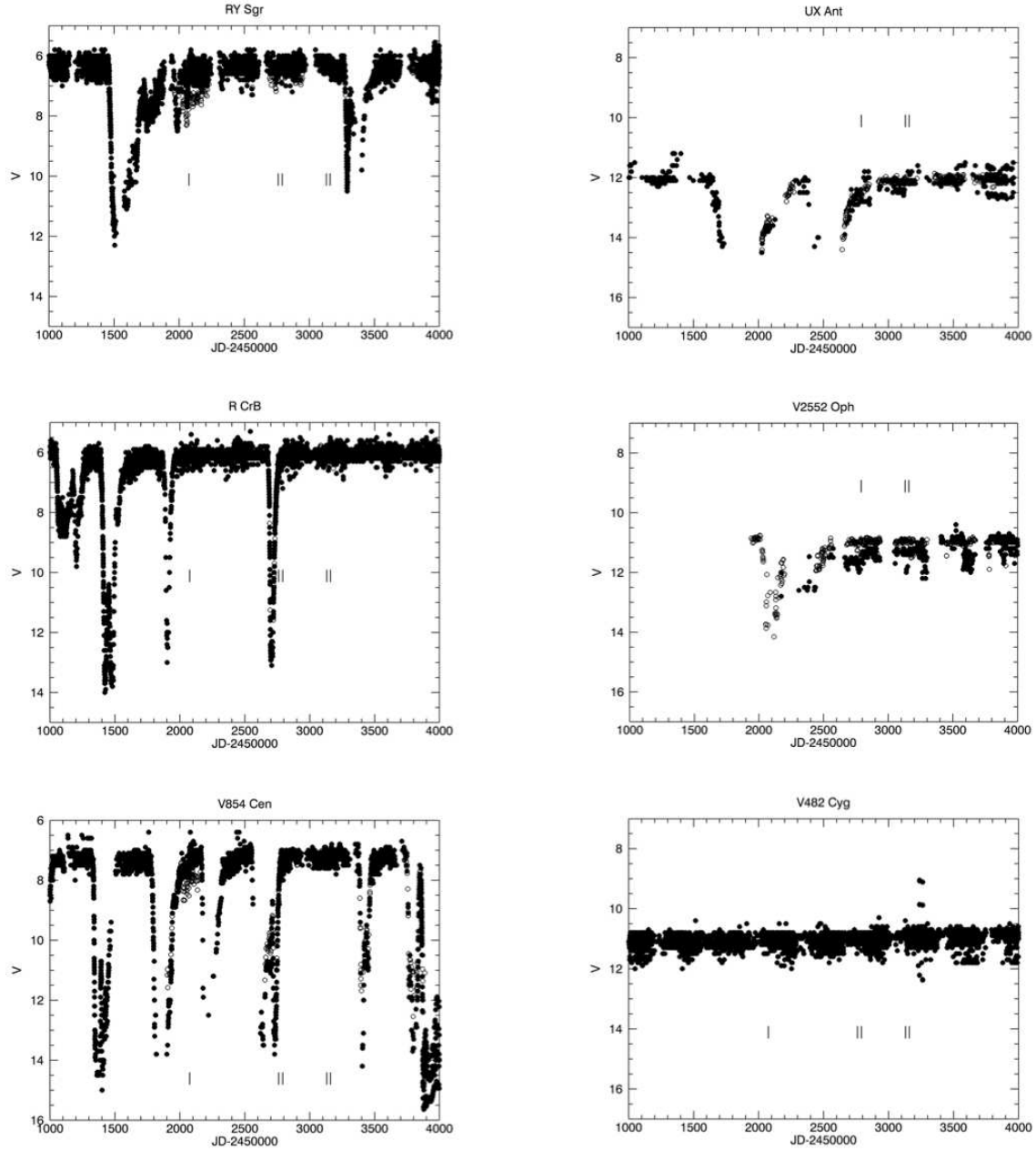


Fig. 2a.— AAVSO (filled circles) and ASAS-3 (open circles) photometry of the sample RCB stars. The epochs of the He I spectra, listed in Table 1, are marked by vertical lines.

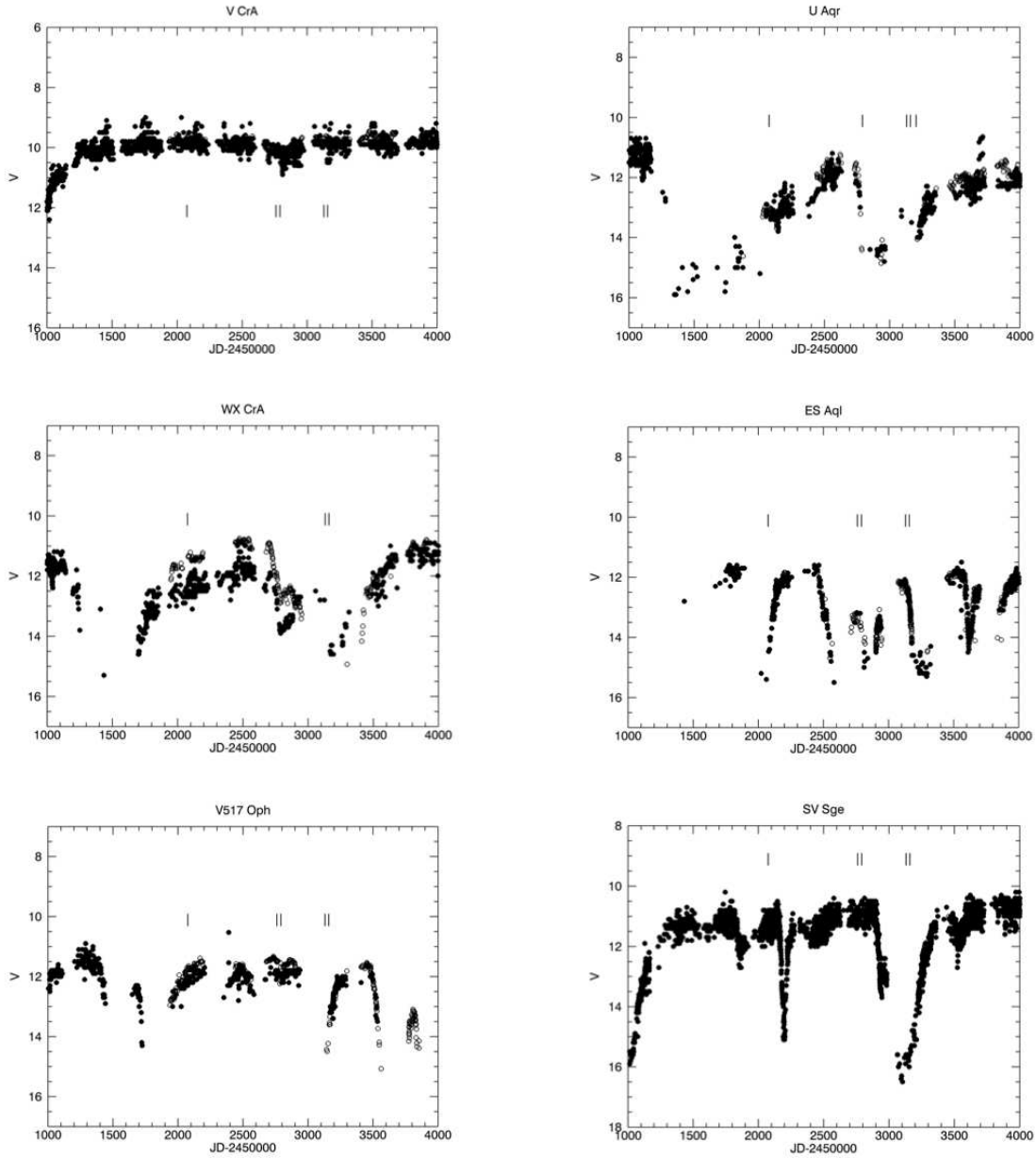


Fig. 2b.— AAVSO (filled circles) and ASAS-3 (open circles) photometry of the sample RCB stars. The epochs of the He I spectra, listed in Table 1, are marked by vertical lines.

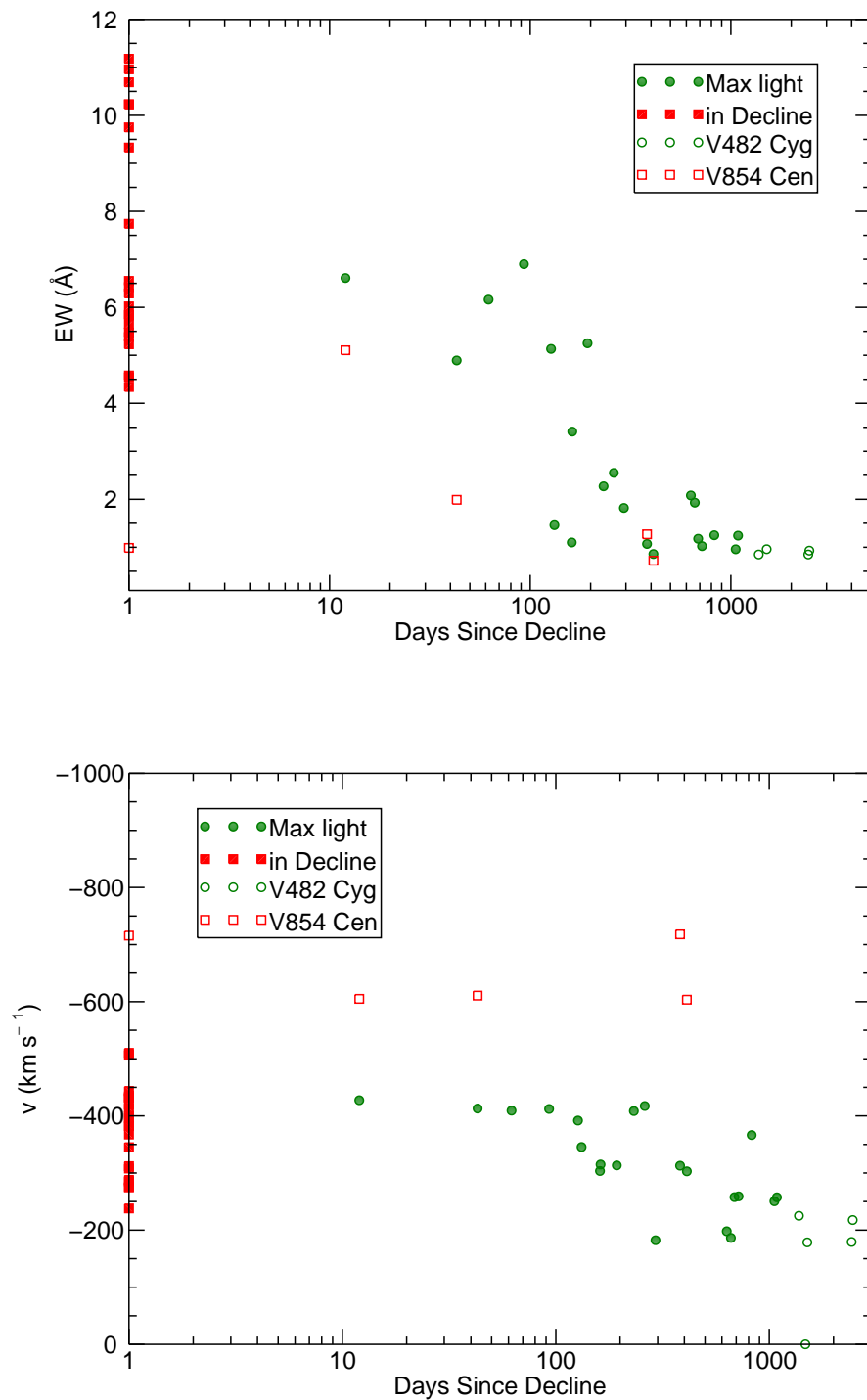


Fig. 3.— Measured equivalent widths (top) and terminal velocities (bottom) of the P-Cygni absorption trough, for each epoch of the twelve stars listed in Table 1, plotted against time in days since the end of the most recent decline. Data points plotted at Day 1 are values observed during declines. Filled symbols are measurements for all stars except V482 Cyg and V854 Cen.